Universal Modulation Scheme to Suppress Transient DC Bias Current in Dual Active Bridge Converters

Shujun Mu, Zhiqiang Guo, *Member, IEEE*, and Yong Luo

***Abstract*—This article presents a modulation scheme to suppress the transient dc bias current in dual active bridge (DAB) converters. The current in the transformer at the commutating time is associated with the initial current in a switching period, so there must be a dc bias current during the transient response. To investigate the modulation scheme for suppressing the transient dc bias current, the article reviews the optimal TPS control strategy, which is derived from the zero voltage switching with the minimum current stress in the transformer. By analyzing the dc bias current, the transient dc bias current can be evaluated by the current in the transformer at the symmetry line of the primary full-bridge voltage waveform instead of the current at the commutating time. It can be concluded that the expressions of the transient dc bias current for different working modes are unified. Therefore, the modulation schemes without transient dc bias current for different working modes can be also unified. On this basis, a universal strategy can meet all the transient cases. There is no need to identify or select the working modes and power conditions in the transient dc bias current control, which simplifies the implementation of the modulation scheme in the digital signal processor. Finally, an experimental prototype has been built to verify the effectiveness of the proposed modulation scheme.**

***Index Terms*—Dual active bridge (DAB), optimal working modes, transient dc bias current.**

I. Introduction

DUAL active bridge (DAB) converter possesses bidirectional power transfer capacity, so it becomes a universal solution for energy storage systems with the galvanic isolation requirement [1], [2]. Fig. 1(a) shows the circuit of the DAB converters, which consists of two full bridges linked with a transformer and a series inductor.

The bidirectional power flow in DAB converters is controlled by the phase shift between the voltages of the two full bridges. The prevalent modulation scheme is the single-phase shift (SPS), where the voltages of the two full bridges are two-level square waveforms [3]. When the input or output voltage varies in a wide range, the converter may work in hard switching and large conduction loss. Therefore, the DAB converters in SPS cannot achieve high efficiency in a wide conversion ratio. To reduce the conduction loss, other modulation schemes are proposed, such as dual-phase shift (DPS) [4], extended-phase shift [5], and triple-phase shift (TPS) [6]. In these modulation schemes, one or two full bridges are three-level waveforms. The equivalent circuit of the DAB converter is shown in Fig. 1(b). By regulating the duty cycle of the two full bridges and the phase shift angle, the conduction loss and the zero voltage switching (ZVS) performance can be optimized. In DPS, the power loss including conduction loss, switching loss, and core loss is set as the optimized objective and solved by using Lagrange multiplier [7]. An optimal DPS is derived for high efficiency. The offline data is stored in the digital signal processor (DSP) to get the optimized working modes. To simplify the optimal DPS control, the peak current in the transformer is set as the optimized target [8]. In this method, an analytical solution is obtained, which makes the modulation scheme flexible. However, some switches in DPS cannot achieve ZVS, which causes more switching loss. An EPS with an auxiliary inductor is proposed for low switching loss in a wide voltage range [9]. In light loads, the EPS control causes a large circulating current, which degrades the efficiency in light loads. DPS and EPS are local optimal modulation schemes [10]. To get the global optimal working mode with low conduction loss, a triple-phase shift (TPS) modulation scheme is investigated to optimize the efficiency for different power loads [10], [11]. The optimization is solved by Karush–Kuhn–Tucker (KKT) or Lagrange multiplier method. In light loads, the converter works in triangular current modulation (TCM). In medium and heavy loads, the converter works in EPS. To extend the wide ZVS and low conduction loss, a modulation scheme with seamless transitions is proposed [12]. As all the switches work in ZVS with minimum conduction loss, the efficiency in light loads is improved. All the above analysis for DAB converters is based on the piecewise linear method. To simplify the analysis, a Fourier-based method has been developed [13]. The current stress and the power are calculated by using fundamental and low-order harmonic components. According to the Fourier-based method, an optimization objective construction method and hybrid optimization algorithm are proposed to calculate the optimal control coordinate [14]. In [15], a particle swarm optimization method is developed for minimum reactive power in DAB converters.

Most of the control strategies for DAB converters are based on single-loop control. The dynamic response is only determined

Manuscript received March 21, 2021; revised June 10, 2021; accepted August 10, 2021. Date of publication August 13, 2021; date of current version October 15, 2021. This work was supported by the National Natural Science Foundation of China under Grant 51807007. Recommended for publication by Associate Editor D. Xu. *(Corresponding author: Zhiqiang Guo.)*

Shujun Mu is with the National Institute of Clean and Low Carbon Energy, Beijing 102211, China (e-mail: shujun.mu.a@chnenergy.com.cn).

Zhiqiang Guo and Yong Luo are with the School of Automation, Beijing Institute of Technology, Beijing 100081, China (e-mail: guozq32@bit.edu.cn; 3120190915@bit.edu.cn).

Color versions of one or more figures in this article are available at https://doi.org/10.1109/TPEL.2021.3104628.

Digital Object Identifier 10.1109/TPEL.2021.3104628

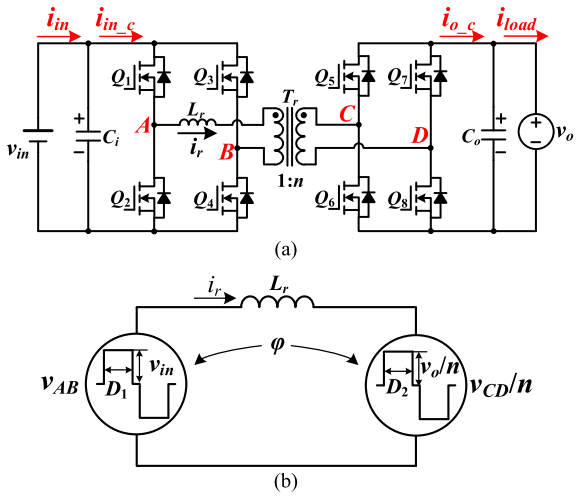

Fig. 1. DAB converter. (a) Circuit of the DAB converter. (b) Equivalent circuit.

by voltage error. Because of the zero-order holder and transport delay in digital control, the converter with single loop control cannot meet the fast dynamic response requirement [16]. To improve the dynamic response, a feedforward compensation based on offline calculation is proposed [16]. The lookup table is stored in the digital signal processor to face the dynamic response. Another phase estimator is proposed as a feedforward path [17]. Virtual direct power control is developed for fast dynamic response [18], [19]. This scheme also can be regarded as a feedforward control, which is determined by the balance of the input and output power. All these feedforward controls are based on the average model in a switching period. The transient state in a switching period is ignored in the analysis. The voltage-second product may not be equal to zero during the fast transient response. In this case, it will cause a large transient dc bias current. A transient phase shift strategy is proposed to reduce the dc bias current [20]. The current in the transformer can be responded in a switching period without the dc bias current. This method is only suitable for SPS and the case where the effective conversion ratio is one. A deadbeat current control is proposed for the fast dynamic response without transient dc bias current [21]. This control strategy is also based on SPS. To reduce the transient dc bias current in a wide voltage range, an improved TPS control strategy is developed for different working mode transitions [22]. The transient case and power change conditions are identified and selected during the transient. In [23], an improved EPS control is proposed to suppress the dc bias current. Magnetic balancing based method is also available to suppress the transient dc bias current [24]. However, an auxiliary circuit is necessary to detect the flux of the transformer. The average current in the transformer is controlled to zero by regulating the duty cycle of the full bridges [23]. A magnetic ear is used to compensate for the voltage-second product of the transformer [24]. In [25], a TPS control strategy to eliminate the transient dc bias current is proposed. All the above methods to suppress the transient dc bias current are only suitable for a specific modulation scheme. Furthermore, they are difficult to extend to the TPS with the optimal working modes with ZVS and low conduction loss.

In all the previous work, the transient dc bias current in DAB converters is evaluated by the current in the transformer at the commutating time. If the converter works in multiple working modes, the control algorithms to eliminate the transient dc bias current are different. To achieve high efficiency in the wide conversion ratio, the DAB converter has to work in multiple working modes. Therefore, the mode selection, the switching pattern, or the power condition should be identified for the different transient states in the transient dc bias current control. In [22], the mode selection should be implemented to suppress the transient dc bias current. The control strategy to eliminate the transient dc bias current in [25] cannot achieve ZVS for all the switches, so it cannot achieve high efficiency in the wide conversion ratio. To face the transient states in different working modes, a state machine is designed in [26]. The switching pattern is designed to determine the transient cases in [27]. To suppress the transient dc bias current for the multiple working modes, the different control strategies are designed for the different working modes, which complicate the implementation of the control strategy.

This article focuses on the suppression of the dc bias current in the transient response. According to the analyses, the currents in the transformer at the symmetry line of the primary full-bridge voltage waveform for different working modes have the same expression. The transient dc bias current can be evaluated by the current in the transformer at the symmetry line of the primary full-bridge voltage waveform instead of the current at the commutating time. Therefore, the control strategies to eliminate the transient dc bias current can be unified. There is no need to select the working modes or the switching pattern, which simplifies the implementation of the control strategy. This is the contribution of this article.

The article is organized as follows. In Section II, the optimal TPS strategy is reviewed, and the optimal working modes are derived and analyzed. In Section III, the dc bias currents for the different optimal working modes are analyzed. The modulation scheme to suppress the dc bias current is proposed. Based on the strategy for the different working modes, a universal control strategy and implementation are presented. Section IV gives the experimental results, which verify the analysis and modulation scheme. Finally, Section V concludes this article.

II. Review of TPS With ZVS and Minimum Peak Current Working Mode for DAB Converters

The duty cycle of the two full bridges and the phase shift angle in DAB converters can be used to optimize the conduction loss. By using the KKT or Lagrange multiplier method [10]–[12], the peak current or the rms current and the ZVS conditions are set as the optimized objectives. The global optimal working mode for the TPS control with ZVS for all the switches and minimum current stress is derived as shown in Fig. 2, where the conversion ratio is defined as $M = V_o/(nV_{\rm in})$. V_o and $V_{\rm in}$ are the quiescent values of v_o and $v_{\rm in}$, they are obtained by using low pass filters. D_1 and D_2 are the duty cycles of the two full bridges, and φ is

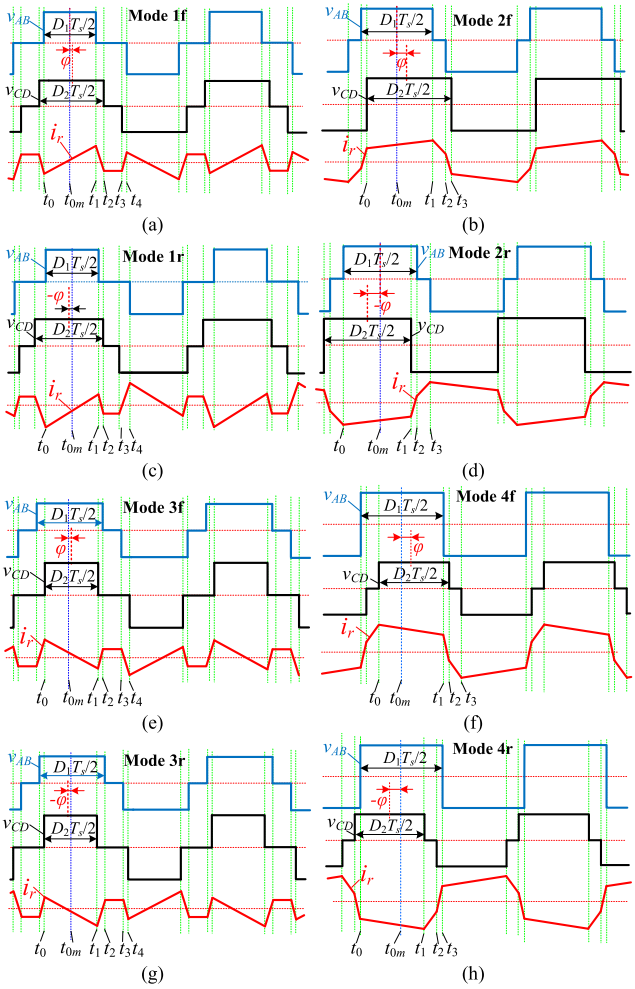

Fig. 2. Key waveforms DAB converter. (a) Mode 1f. (b) Mode 2f. (c) Mode 1r. (d) Mode 2r. (e) Mode 3f. (f) Mode 4f. (g) Mode 3r. (h) Mode 4r.

the phase shift angle. T_s is the switching period. Fig. 2(a) and (b) shows the working modes for the forward power flow when M is less than 1. Fig. 2(c) and (d) shows the working modes for the reverse power flow when M is less than 1. Fig. 2(e) and (f) shows the working modes for the forward power flow when M is larger than 1. Fig. 2(g) and (h) shows the working modes for the reverse power flow when M is larger than 1. Fig. 2(a), (c), (e), and (g) corresponds to the light load, and Fig. 2(b), (d), (f), and (h) corresponds to the heavy load.

According to the symmetrical current waveforms in the steady state, the currents of the transformer can be calculated. As seen in Fig. 2, the time at t_{0m} in Fig. 2 is defined as the symmetry line of v_{AB} in a switching period. The current at t_{0m} in all the working modes in Fig. 2, including both cases of $M \geq 1$ and $M < 1$, is shown in (1). The detailed derivation can be referred to in the Appendix

$$i_r(t_{0m}) = \frac{V_o T_s}{4nL_r}\left(\frac{2\varphi}{\pi}\right). \tag{1}$$

For all the working modes in Fig. 2, the current of the transformer at the time of t_{0m} in the steady state is associated with φ but independent of D_1 and D_2. The phase shift angle and the output voltage can determine the current in the transformer of the symmetry line of v_{AB} in a switching period. In all the previous works, the dc bias current is evaluated by the current at the commutating time, so the equations to evaluate the dc bias current are different for different working modes. This article reveals the relationship between the phase shift angle and the current in the transformer at the symmetry line of v_{AB}. According to this relationship, the transient dc bias current can be evaluated according to (1). Therefore, the transient dc bias currents for the working modes in Fig. 2 have the same expression, which will be analyzed in detail in Section III.

To optimize the ZVS and conduction loss in the DAB converter, the global optimal working modes can be derived in terms of Lagrange multiplier or KKT theory [10], [12]. Setting the peak current as the optimized objective, the duty cycles of the two full bridges can be calculated by the phase shift angle φ. In different working modes in Fig. 2, they are shown in (2) to (5), where $\varphi_s = 2\varphi/\pi$. I_{ZVS1} is the minimum current amplitude for the ZVS of Q_1–Q_4, while I_{ZVS2} is the minimum current amplitude for the ZVS of Q_5–Q_8. If D_1 or D_2 in the algorithm of (2) to (5) is larger than one, D_1 or D_2 is set equal to one. The method to derive (2) to (5) is shown in the Appendix

$$\begin{cases} D_1 = \frac{M}{1-M}\left(|\varphi_s| + \frac{4L_r I_{\mathrm{ZVS1}}}{V_{in}T_s}\right) \\ D_2 = \frac{D_1}{M} + \frac{4nL_r I_{\mathrm{ZVS2}}}{V_o T_s} \end{cases}$$

$$0 \leq |\varphi_s| \leq 1 - M \& M < 1 \,(\text{Mode1f and Mode1r}) \tag{2}$$

$$\begin{cases} D_1 = \frac{2M-1}{M} + \frac{1-M}{M}|\varphi_s| \\ D_2 = 1 \end{cases}$$

$$1 - M < |\varphi_s| \leq 1 \& M < 1 \,(\text{Mode2f and Mode2}r) \tag{3}$$

$$\begin{cases} D_2 = \frac{1}{M-1}\left(|\varphi_s| + \frac{4L_r I_{\mathrm{ZVS2}}}{V_{in}T_s}\right) \\ D_1 = MD_2 + \frac{4L_r I_{\mathrm{ZVS1}}}{V_{in}T_s} \end{cases}$$

$$0 \leq |\varphi_s| \leq 1 - \frac{1}{M} \& M \geq 1 \,(\text{Mode3f and Mode3r}) \tag{4}$$

$$\begin{cases} D_2 = (2-M) + (M-1)|\varphi_s| \\ D_1 = 1 \end{cases}$$

$$1 - \frac{1}{M} < |\varphi_s| \leq 1 \& M \geq 1 \,(\text{Mode4f and Mode4}r)\,. \tag{5}$$

III. Modulation Scheme to Suppress the Transient DC Bias Current

A. Transient DC Bias Current Issue

The experimental results for the transient response are shown in Fig. 3, where $V_{\mathrm{in}} = 200$ V, $V_o = 200$ V, $n = 1$, $L_r = 80$ μH, $C_o = 20$ μF, and $T_s = 20$ μs. In this case, the conversion ratio is one, so D_1 and D_2 are both equal to one according to the control law in (2) to (5). Therefore, the converter works in SPS, which also can be viewed as a specific working mode in the TPS control. When the phase shift angle in the DAB converter is regulated in a very slow dynamic response for the output voltage closed-loop control, the average voltage across the series inductor in a

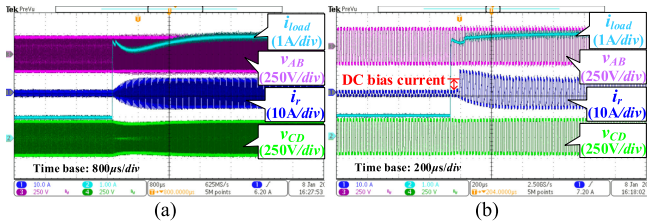

Fig. 3. Transient response with the SPS control. (a) Slow dynamic response. (b) Fast dynamic response.

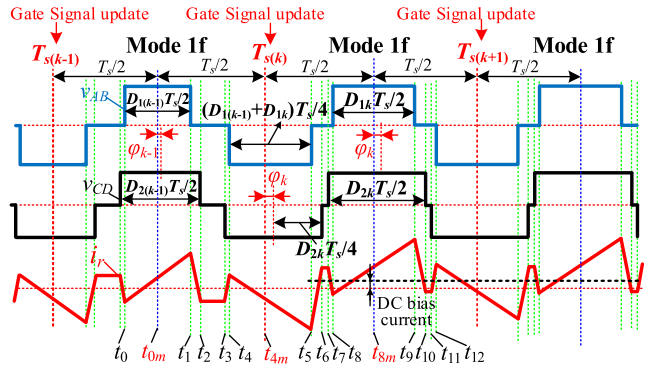

Fig. 4. Waveforms of Mode 1f in the transient state.

switching period is nearly equal to zero all the time. Therefore, there is no dc bias current during the transient response, as shown in Fig. 3(a). Because the gate signals of the switches are updated once in a switching period for the digital controllers, the current in the transformer at the commutating time is associated with the initial current in a switching period. As shown in Fig. 3(b), when the converter is regulated in a fast dynamic response, it will cause a large dc bias current during the transient. Although the dc bias current can be damped by the internal resistance of the converter after a while, it may cause the overcurrent of the switches or the saturation of the transformer and inductor. The detailed dc bias current of the optimized working mode in Section II will be analyzed in the following section.

B. Mode 1f and Mode 1r

The waveforms of Mode 1f in the transient state are shown in Fig. 4. In the digital controller, the gate signals of the switches are updated once in a switching period, i.e., updated at the time of $T_{s(k)}$, where $k = 0, 1, 2\ldots$. As seen in Fig. 4, the duty cycle of the full bridges and the phase shift angle are updated at the time of $T_{s(k)}$. From $T_{s(k)}$ to $T_{s(k+1)}$, the duty cycle of the two full bridges and the phase shift angle is designated as D_{1k}, D_{2k}, and φ_k, which meet the relationship in (2). At the time of t_{4m}, the phase shift angle is switched from $\varphi_{k\text{-}1}$ to φ_k.

The line at the time of t_{8m} is the symmetry line of v_{AB} during $T_{s(k)}$ to $T_{s(k+1)}$. The current at t_{8m} is expressed in (6), where v_{Lr} is the voltage across the series inductor

$$i_r(t_{8m}) = i_r(t_{4m}) + \frac{1}{L_r}\int_{t_{4m}}^{t_{8m}} v_{Lr}dt$$
$$= i_r(t_{4m}) + \frac{-V_{\text{in}} + V_o/n}{L_r}(t_5 - t_{4m})$$

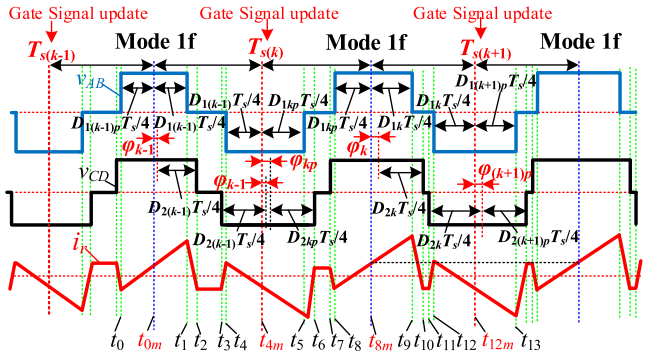

Fig. 5. Waveforms of Mode 1f in the transient state without dc bias current.

$$+\frac{V_o/n}{L_r}(t_6 - t_5) - \frac{V_o/n}{L_r}(t_8 - t_7)$$
$$+\frac{V_{\text{in}} - V_o/n}{L_r}(t_{8m} - t_8)$$
$$= -\frac{V_o T_s}{4nL_r}\left(\frac{2\varphi_{k-1}}{\pi}\right) + \frac{-V_{\text{in}} + V_o/n}{L_r}D_{1k}\frac{T_s}{4}$$
$$+\frac{V_o/n}{L_r}\left(D_{2k} + \frac{2\varphi_k}{\pi} - D_{1k}\right)\frac{T_s}{4}$$
$$-\frac{V_o/n}{L_r}\left(D_{2k} - \frac{2\varphi_k}{\pi} - D_{1k}\right)\frac{T_s}{4}$$
$$+\frac{V_{\text{in}} - V_o/n}{L_r}D_{1k}\frac{T_s}{4}$$
$$= \frac{V_o T_s}{4nL_r}\left(\frac{2\varphi_k}{\pi}\right) + \frac{V_o T_s}{4nL_r}\left(\frac{2(\varphi_k - \varphi_{k-1})}{\pi}\right). \quad (6)$$

According to (1), the current at the symmetry line of v_{AB} in the steady state is equal to $\frac{V_o T_s}{4nL_r}(\frac{2\varphi_k}{\pi})$. Therefore, the dc bias current during the transient state in Fig. 4 is evaluated as $\frac{V_o T_s}{4nL_r}(\frac{2(\varphi_k - \varphi_{k-1})}{\pi})$. The dc bias current is only associated with the error of the phase shift angle between the two adjacent switching periods. If φ_k is larger than $\varphi_{k\text{-}1}$, the dc bias current in Mode 1f is positive, and vice versa.

As seen in Fig. 5, the phase shift angle is updated at the time $T_{s(k)}$. Due to the symmetry of the waveforms, the current in the transformer at t_{4m} is expressed as $-\frac{V_o T_s}{4nL_r}(\frac{2\varphi_{k-1}}{\pi})$. Assuming the current in the transformer at the symmetry line between $T_{s(k)}$ and $T_{s(k+1)}$, i.e., the current at t_{8m}, is equal to $\frac{V_o T_s}{4nL_r}(\frac{2\varphi_k}{\pi})$, the dc bias during the transient state between $T_{s(k)}$ to $T_{s(k+1)}$ must be eliminated. In this case, the phase shift angle and the duty cycle of the two full bridges between t_{4m} to t_{8m} are defined as φ_{kp}, D_{1kp}, and D_{2kp}. The relationship of φ_{kp}, D_{1kp}, and D_{2kp} also meet the equation in (2). The following expression is satisfied:

$$i_r(t_{8m}) = i_r(t_{4m}) + \frac{1}{L_r}\int_{t_{4m}}^{t_{8m}} v_{Lr}dt$$
$$= i_r(t_{4m}) + \frac{-V_{\text{in}} + V_o/n}{L_r}(t_5 - t_{4m}) + \frac{V_o/n}{L_r}(t_6 - t_5)$$
$$-\frac{V_o/n}{L_r}(t_8 - t_7) + \frac{V_{\text{in}} - V_o/n}{L_r}(t_{8m} - t_8)$$

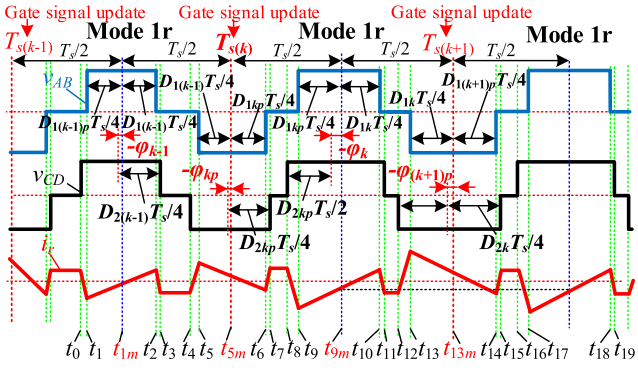

Fig. 6. Waveforms of Mode 1r in the transient state without dc bias current.

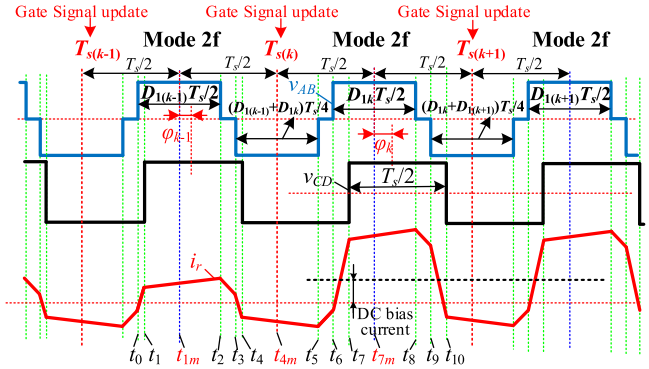

Fig. 7. Waveforms of Mode 2f in the transient state.

$$= -\frac{V_o T_s}{4nL_r}\left(\frac{2\varphi_{k-1}}{\pi}\right) + \frac{-V_{\text{in}} + V_o/n}{L_r} D_{1kp}\frac{T_s}{4} + \frac{V_o/n}{L_r}\left(D_{2kp} + \frac{2\varphi_{kp}}{\pi} - D_{1kp}\right)\frac{T_s}{4} - \frac{V_o/n}{L_r}\left(D_{2kp} - \frac{2\varphi_{kp}}{\pi} - D_{1kp}\right)\frac{T_s}{4} + \frac{V_{\text{in}} - V_o/n}{L_r} D_{1kp}\frac{T_s}{4}$$
$$= -\frac{V_o T_s}{4nL_r}\left(\frac{2\varphi_{k-1}}{\pi}\right) + \frac{V_o T_s}{2nL_r}\left(\frac{2\varphi_{kp}}{\pi}\right). \quad (7)$$

If $i_r(t_{8m})$ is equal to $\frac{V_o T_s}{2nL_r}(\frac{2\varphi_k}{\pi})$, the dc bias current must be eliminated. Therefore, φ_{kp} is derived in (8)

$$-\frac{V_o T_s}{4nL_r}\left(\frac{2\varphi_{k-1}}{\pi}\right) + \frac{V_o T_s}{2nL_r}\left(\frac{2\varphi_{kp}}{\pi}\right) = \frac{V_o T_s}{2nL_r}\left(\frac{2\varphi_k}{\pi}\right)$$
$$\Rightarrow \varphi_{kp} = \frac{\varphi_k + \varphi_{k-1}}{2}. \quad (8)$$

As seen in Fig. 5, the phase shift angle during t_{8m}–t_{12m} is equal to φ_k. Equation (8) shows that the phase shift angle during t_{4m}–t_{8m} is associated with both of the two adjacent switching periods. Therefore, the working mode during t_{4m}–t_{8m} can be regulated as an intermediate working mode during the transient state without transient dc bias current.

This method is also effective for Mode 1r. The waveforms in Mode 1r are shown in Fig. 6. The phase shift angle is changed from φ_{k-1} to φ_k during $T_{s(k)}$ to $T_{s(k+1)}$, where φ_{k-1} and φ_k are the negative for the reverse power flow. The phase shift angle and the duty cycle of the two full bridges between t_{5m} and t_{9m} are defined as φ_{kp}, D_{1kp}, and D_{2kp}. If the current at t_{9m} is equal to $\frac{V_o T_s}{4nL_r}(\frac{2\varphi_k}{\pi})$. The dc bias current is eliminated. In this case, the following condition is satisfied:

$$i_r(t_{9m}) = i_r(t_{5m}) + \frac{1}{L_r}\int_{t_{5m}}^{t_{9m}} v_{Lr}dt$$
$$= i_r(t_{5m}) + \frac{-V_{\text{in}} + V_o/n}{L_r}(t_6 - t_{5m}) + \frac{V_o/n}{L_r}(t_7 - t_6) - \frac{V_o/n}{L_r}(t_9 - t_8) + \frac{V_{\text{in}} - V_o/n}{L_r}(t_{9m} - t_9)$$
$$= -\frac{V_o T_s}{4nL_r}\left(\frac{2\varphi_{k-1}}{\pi}\right) + \frac{V_o T_s}{2nL_r}\left(\frac{2\varphi_{kp}}{\pi}\right)$$
$$= \frac{V_o T_s}{4nL_r}\left(\frac{2\varphi_k}{\pi}\right). \quad (9)$$

According to (9), the following expression is also derived by the same method as Mode 1f

$$\varphi_{kp} = \frac{\varphi_k + \varphi_{k-1}}{2}. \quad (10)$$

It is expressed the same as (8). Therefore, the methods to suppress the transient dc bias current for Mode 1f and Mode 1r are the same.

C. Mode 2f and Mode 2r

The waveforms of Mode 2f in the transient state with dc bias current are shown in Fig. 7, where the phase shift angle is switched from φ_{k-1} to φ_k at t_{4m}. The duty cycles and phase shift angle are designated the same as the analysis in Mode 1f. According to (1) and the symmetry of the current waveform in the steady state, the current at t_{4m} is expressed as $-\frac{V_o T_s}{4nL_r}(\frac{2\varphi_{k-1}}{\pi})$. Therefore, the current at t_{7m} is expressed in (11). In the steady state, the current at the symmetry line of v_{AB} in Mode 2f is expressed as $\frac{V_o T_s}{4nL_r}(\frac{2\varphi_k}{\pi})$. Therefore, the dc bias current during the transient state is evaluated as $\frac{V_o T_s}{4nL_r}(\frac{2(\varphi_k - \varphi_{k-1})}{\pi})$, which is the same as the expression of the dc bias current for Mode 1f

$$i_r(t_{7m}) = i_r(t_{5m}) + \frac{1}{L_r}\int_{t_{4m}}^{t_{7m}} v_{Lr}dt$$
$$= i_r(t_{4m}) + \frac{-V_{\text{in}} + V_o/n}{L_r}(t_5 - t_{4m}) + \frac{V_o/n}{L_r}(t_6 - t_5) + \frac{V_{\text{in}} + V_o/n}{L_r}(t_7 - t_6) + \frac{V_{\text{in}} - V_o/n}{L_r}(t_{7m} - t_7)$$
$$= \frac{V_o T_s}{4nL_r}\left(\frac{2\varphi_k}{\pi}\right) + \frac{V_o T_s}{4nL_r}\left(\frac{2(\varphi_k - \varphi_{k-1})}{\pi}\right). \quad (11)$$

If the current in the transformer at the symmetry line of v_{AB} is equal to $\frac{V_o T_s}{4nL_r}(\frac{2\varphi_k}{\pi})$, i.e., the current at t_{7m} in Fig. 8 is equal to $\frac{V_o T_s}{4nL_r}(\frac{2\varphi_k}{\pi})$, the dc bias current during the transient state is eliminated. As seen in Fig. 8, the phase shift angle and the duty

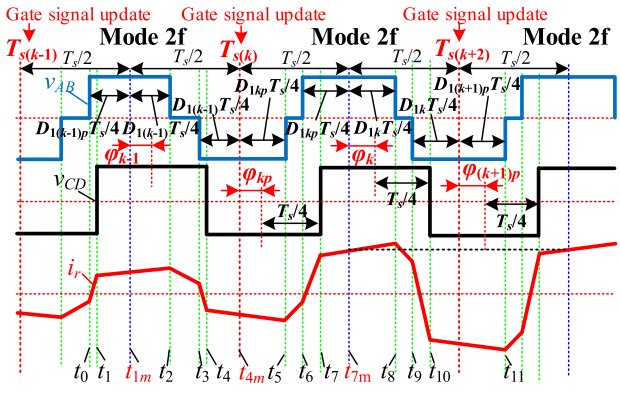

Fig. 8. Waveforms of Mode 2f in the transient state without dc bias current.

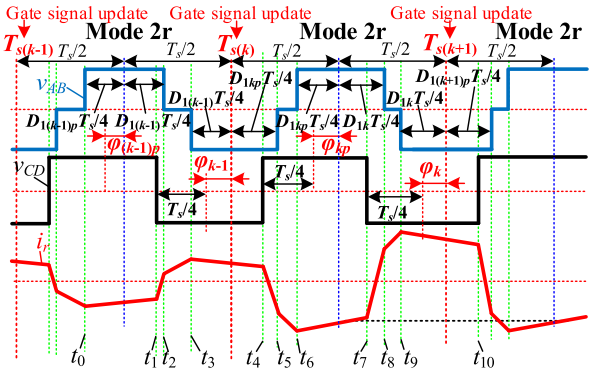

Fig. 9. Waveforms of Mode 2r in the transient state without dc bias current.

cycle of the two full bridges between t_{4m} and t_{7m} are also defined as φ_{kp}, D_{1kp}, and D_{2kp}. The relationship of φ_{kp}, D_{1kp}, and D_{2kp} for Mode 2f meets the equation in (3). As seen in Fig. 8, the following expression is satisfied:

$$\begin{aligned} i_r(t_{7m}) &= i_r(t_{4m}) + \frac{1}{L_r}\int_{t_{5m}}^{t_{7m}} v_{Lr}dt \\ &= i_r(t_{4m}) + \frac{V_o/n - V_{\text{in}}}{L_r}(t_5 - t_{4m}) + \frac{V_o/n}{L_r}(t_6 - t_5) \\ &\quad + \frac{V_{\text{in}} + V_o/n}{L_r}(t_7 - t_6) + \frac{V_{\text{in}} - V_o/n}{L_r}(t_{7m} - t_7) \\ &= -\frac{V_o T_s}{4nL_r}\left(\frac{2\varphi_{k-1}}{\pi}\right) + \frac{V_o T_s}{2nL_r}\left(\frac{2\varphi_{kp}}{\pi}\right). \end{aligned} \tag{12}$$

If $i_r(t_{7m})$ is equal to $\frac{V_o T_s}{2nL_r}(\frac{2\varphi_k}{\pi})$, the dc bias current must be eliminated. Therefore, φ_{kp} is derived in (13), which is the same as the expression for Mode 1f and Mode 1r

$$\begin{aligned} &-\frac{V_o T_s}{4nL_r}\left(\frac{2\varphi_{k-1}}{\pi}\right) + \frac{V_o T_s}{2nL_r}\left(\frac{2\varphi_{kp}}{\pi}\right) \\ &= \frac{V_o T_s}{2nL_r}\left(\frac{2\varphi_k}{\pi}\right) \Rightarrow \varphi_{kp} = \frac{\varphi_k + \varphi_{k-1}}{2}. \end{aligned} \tag{13}$$

The transient state without dc bias current for Mode 2r is shown in Fig. 9. The method to suppress the dc bias current can be derived according to the same analyses. Therefore, φ_{kp} for Mode 2r is expressed the same as (13).

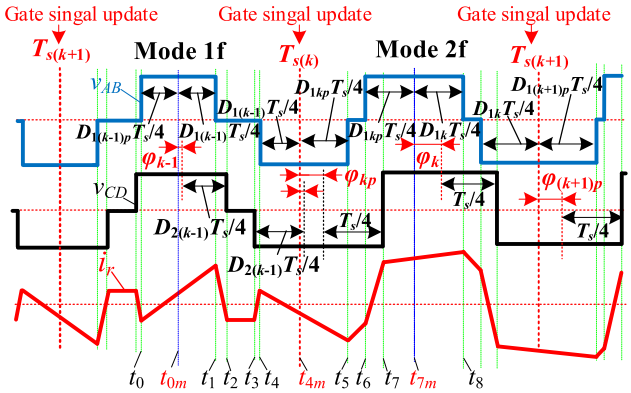

Fig. 10. Waveforms of the transition from Mode 1f to Mode 2f in the transient state without dc bias current.

D. Working Mode Transition Between Mode 1f and Mode2f

When the converter is switched from Mode 1f to Mode2f, the current in the transformer also has dc bias current during the transient state. The bias current amplitude is the same as the analyses in Mode 1f and Mode 2f. The transition from Mode 1f to Mode 2f without the transient dc bias current is shown in Fig. 10. The phase shift angle is changed from $\varphi_{k\text{-}1}$ to φ_k at t_{4m}. Before t_{4m}, the converter works in the steady state, so the current at $t_{4\text{m}}$ is expressed as $-\frac{V_o T_s}{4nL_r}(\frac{2\varphi_{k-1}}{\pi})$. If the current at the time of t_{7m} is expressed as $\frac{V_o T_s}{4nL_r}(\frac{2\varphi_k}{\pi})$, the transient dc bias current can be eliminated. The condition in (14) is satisfied. Rewriting (14), the same expression as (10) and (13) is derived. If the working mode converts from Mode 2f to Mode 1f, the same conclusion can be derived

$$\begin{aligned} i_r(t_{7m}) &= i_r(t_{4m}) + \frac{1}{L_r}\int_{t_{4m}}^{t_{7m}} v_{Lr}dt \\ &= i_r(t_{4m}) + \frac{V_o/n - V_{\text{in}}}{L_r}(t_5 - t_{4m}) + \frac{V_o/n}{L_r}(t_6 - t_5) \\ &\quad + \frac{V_{\text{in}} + V_o/n}{L_r}(t_7 - t_6) + \frac{V_{\text{in}} - V_o/n}{L_r}(t_{7m} - t_7) \\ &= -\frac{V_o T_s}{4nL_r}\left(\frac{2\varphi_{k-1}}{\pi}\right) + \frac{V_o T_s}{2nL_r}\left(\frac{2\varphi_{kp}}{\pi}\right) \\ &= \frac{V_o T_s}{2nL_r}\left(\frac{2\varphi_k}{\pi}\right). \end{aligned} \tag{14}$$

E. Other Working Mode Transitions

Fig. 11 shows the waveform for the other working mode transitions without the transient dc bias current. In Fig. 11(a) to (f), the phase shift angle is switched from $\varphi_{k\text{-}1}$ to φ_k at the time of t_{1m}. The current at $t_{1\,m}$ is equal to $-\frac{V_o T_s}{4nL_r}(\frac{2\varphi_{k-1}}{\pi})$. If there is no dc bias current at the transient state. The current at t_{2m} must be equal to $\frac{V_o T_s}{4nL_r}(\frac{2\varphi_k}{\pi})$, which demonstrates that the analyses are the same as the previous analyses. Therefore, the modulation scheme to suppress the dc bias current during the transient response is the same as the conditions in (8), (10), and (13).

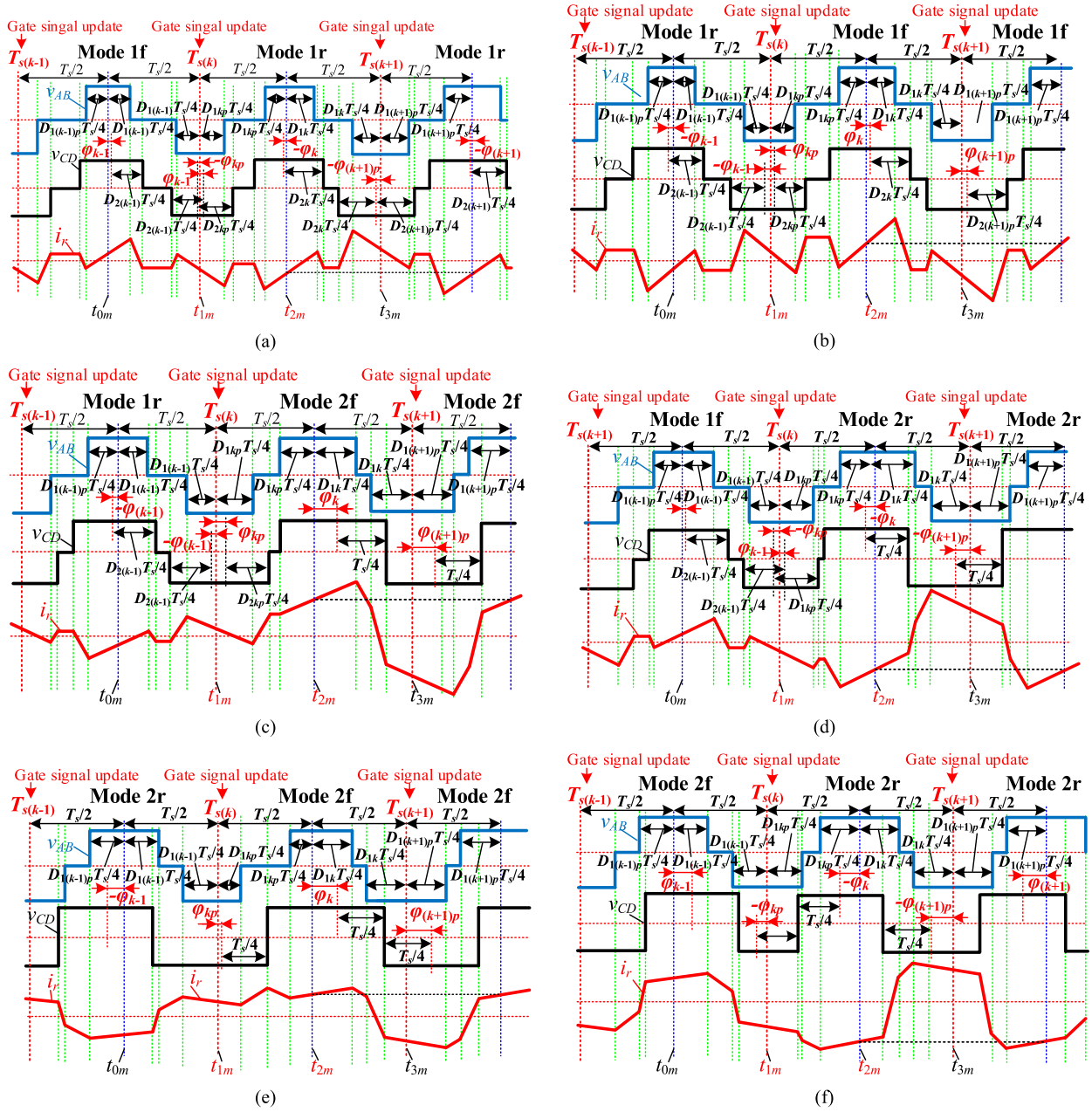

Fig. 11. Waveforms of the working mode transition without dc bias current. (a) From Mode 1f to Mode 1r. (b) From Mode 1r to Mode 1f. (c) From Mode 1r to Mode 2f. (d) From Mode 1f to Mode 2r. (e) From Mode 2r to Mode 2f. (f) From Mode 2f to Mode 2r.

Above all, the modulation scheme to eliminate the transient dc bias current for all the working modes in Fig. 2 is expressed in (13). Therefore, the modulation scheme to eliminate the transient dc bias current for all the working modes in Fig. 2 is unified. There is no need to identify the working modes before and after the transient, which simplifies the implementation of the control strategy. The above analysis is based on when the conversion ratio M is less than 1. By using the same analyses, the constraint in (13) also meets the optimal working mode for $M > 1$. The working modes in Fig. 2 are the global optimal working modes, so TCM, EPS, and SPS are the specific working modes in Fig. 2. Therefore, the proposed universal modulation scheme to suppress the transient dc bias current can be extended to the other modulation scheme including TCM, EPS, and SPS.

F. Implementation of the Modulation Scheme

The gate signal generation is shown in Fig. 12. Taking Q_1 for example, when the PWM1A is equal to the increment counter, Q_1 is set and Q_2 is clear. When the PWM1B is equal to the increment counter, Q_1 is clear and Q_2 is set. Q_1 and Q_2 are supplementary with deadtime. At the commutating times, the deadtime is set to prevent the occurrence of the shoot-through

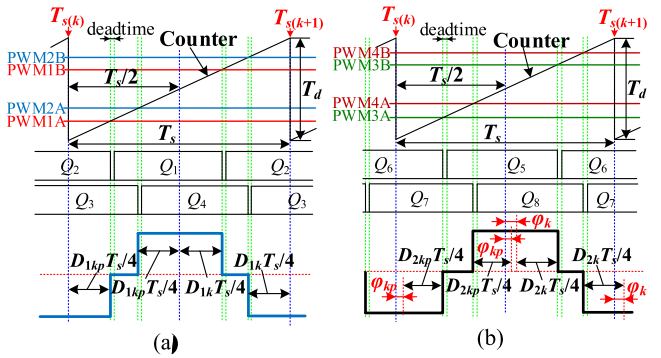

Fig. 12. Gate signal generation: (a) for Q_1–Q_4 and (b) for Q_5–Q_8.

issue. Q_3–Q_8 is generated with the same as Q_1 and Q_2, where T_d is the peak value of the increment counter.

As seen in Fig. 12, the gate signals are updated when the counter is equal to zero. The rising edge of Q_1 and Q_4 is determined by D_{1kp}, and the falling edge of Q_1 and Q_4 is determined by D_{1k}. The rising edge of Q_5 and Q_8 is determined by D_{2kp} and φ_{kp}, and the falling edge of Q_1 and Q_4 is determined by D_{2k} and φ_k. Therefore, the comparative value for generating the gate signal is expressed as (15), where φ_{kp} and φ_k must be in the range from $-\pi/2$ to $\pi/2$. When the converter works in Mode 2f or Mode2r, D_{2k} and D_{2pk} are equal to one. When the converter works in Mode 4f or Mode4r, D_{1k} and D_{1pk} are equal to one. In the steady state, φ_k is equal to $\varphi_{k\text{-}1}$, so φ_{kp} is equal to φ_k. D_{1kp} is equal to D_{1k} in the steady state, while D_{2kp} is also equal to D_{2k}. According to (15), the duty cycle of all the switches is 0.5 in the steady state, which also meets the conventional TPS in the steady-state requirement. Therefore, the equations in (15) meet both the transient state and steady state.

$$\begin{cases} \mathrm{PWM1}A = (0.25 \cdot D_{1kp})\, T_d \\ \mathrm{PWM1}B = (0.5 + 0.25 \cdot D_{1k})\, T_d \\ \mathrm{PWM2}A = (0.5 - 0.25 \cdot D_{1kp})\, T_d \\ \mathrm{PWM2}B = (1 - 0.25 \cdot D_{1k})\, T_d \end{cases}$$

$$\begin{cases} \mathrm{PWM3}A = \left(\frac{\varphi_{kp}}{2\pi} + 0.25 \cdot D_{2kp}\right) T_d \\ \mathrm{PWM3}B = \left(0.5 + \frac{\varphi_k}{2\pi} + 0.25 \cdot D_{2k}\right) T_d \\ \mathrm{PWM4}A = \left(0.5 + \frac{\varphi_{kp}}{2\pi} - 0.25 \cdot D_{2kp}\right) T_d \\ \mathrm{PWM4}B = \left(1 + \frac{\varphi_k}{2\pi} - 0.25 \cdot D_{2k}\right) T_d. \end{cases} \quad (15)$$

The flowchart of the universal modulation scheme to eliminate the transient dc bias current is shown in Fig. 13. φ_k is dynamically set by the controller. According to M and φ_k, D_{1k} and D_{2k} are calculated by (2) to (5). φ_{kp} is calculated by (13), then $\varphi_{k\text{-}1}$ is set as φ_k. According to M and φ_{kp}, D_{1kp}, and D_{2kp} are calculated by (2) to (5). Then, the comparative values are calculated by (15), and the gate signals are generated according to Fig. 12. The flowchart is implemented once in a switching period.

IV. Experimental Validation

An experimental prototype is built to verify the modulation scheme. The detailed specifications are shown in Table I. The control strategy is implemented in a TMS320F28335 DSP. The

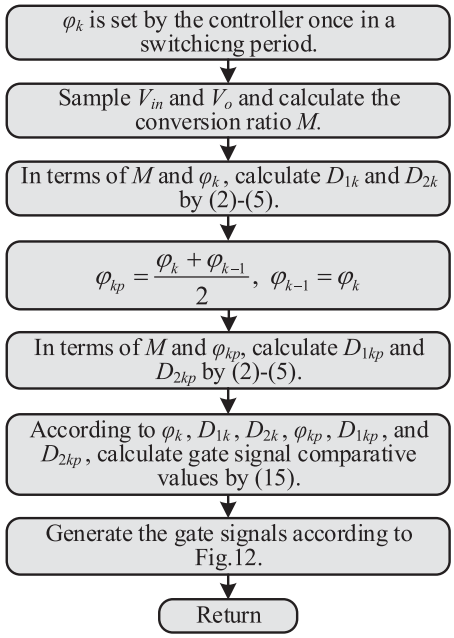

Fig. 13. Flowchart of the modulation scheme.

TABLE I
Detailed Specifications

Items	Symbol	Parameter
Battery voltage	v_{in}	150 V
Output voltage	v_o	100 V
Turns ratio of the transformer	n	1
Switching frequency (period)	$f_s\,(T_s)$	50*k*Hz (20 μs)
Switches	$Q_{1\text{-}8}$	FDA50N50 (FairChild)
Series inductor	L_r	80μH

concept of the test bench is shown in Fig. 14(a). A back-to-back system consists of a DAB converter and a non-isolated buck/boost converter, which both possess bidirectional power transfer capability. The output voltage v_o is controlled by the buck/boost converter. The input voltage is clamped by the power supply. The buck/boost converter regulates the output voltage and circulating the power in the test bench. When the DAB converter transfers power from the input side to the output side, i.e., charging the output voltage, the buck/boost converter is adjusted to transfer power from the output side to the input side for maintaining v_o stability. When the DAB converter transfers power from the output side to the input side, the buck/boost converter will transfer power from the input side to the output side. Fig. 14(b) shows the experimental prototype. In this setup, only one power supply is necessary for testing the DAB converter in bidirectional power transfer.

Fig. 15 shows the transient response in Mode 1f, where the phase shift angle φ is switched from 0.03 π to 0.127 π at the time of t_m. Fig. 15(a) shows the conventional TPS. The current amplitude of the transformer shows the obvious transient dc bias current. Fig. 15(b) shows the improved modulation scheme without dc bias current. The transient procedure is within a

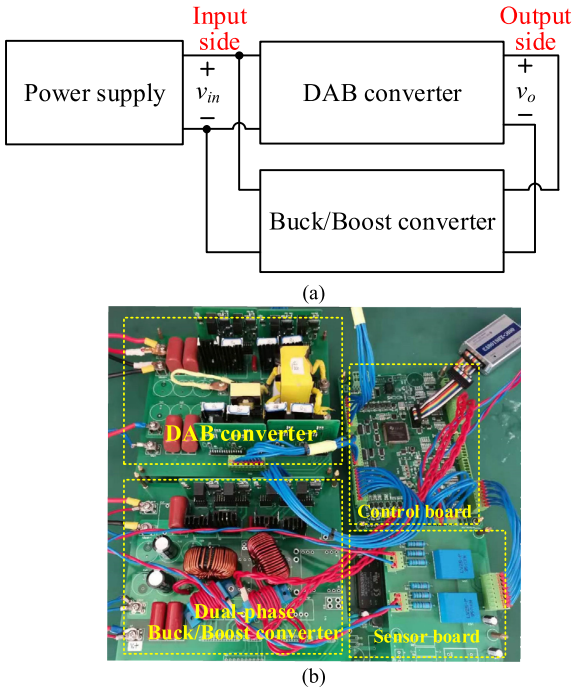

Fig. 14. (a) Concept of the test bench. (b) Experimental prototype.

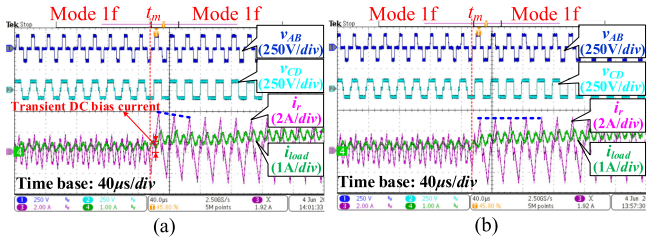

Fig. 15. Transient response in Mode 1f. (a) Conventional TPS. (b) Universal modulation scheme without dc bias current.

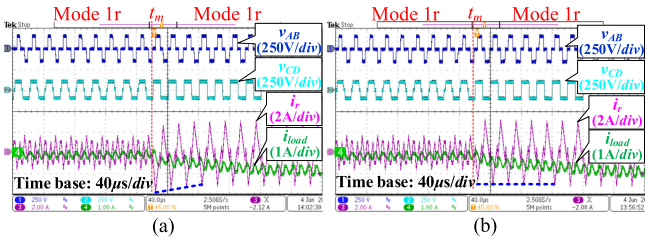

Fig. 16. Transient response in Mode 1r. (a) Conventional TPS. (b) Universal modulation scheme without dc bias current.

switching period. The current amplitude of the transformer after t_m are the same.

Fig. 16 shows the transient response in Mode 1r, where the phase shift angle is switched from $-0.03\ \pi$ to $-0.127\ \pi$ at the time of t_m. In this case, the DAB converter works in reverse power flow. Fig. 16(a) shows the conventional TPS, which shows the transient dc bias current. The transient dc bias current is negative in this case. Fig. 16(b) shows the improved modulation scheme without dc bias current. The transient procedure is also within a switching period. The waveforms are symmetrical with the ones in Fig. 15(b).

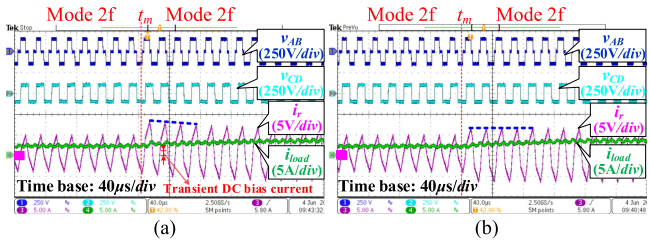

Fig. 17. Transient response in Mode 2f. (a) Conventional TPS. (b) Universal modulation scheme without dc bias current.

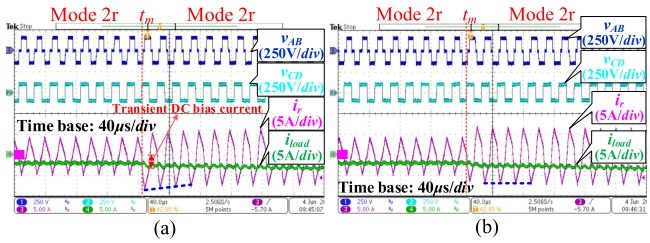

Fig. 18. Transient response in Mode 2r. (a) Conventional TPS. (b) Universal modulation scheme without dc bias current.

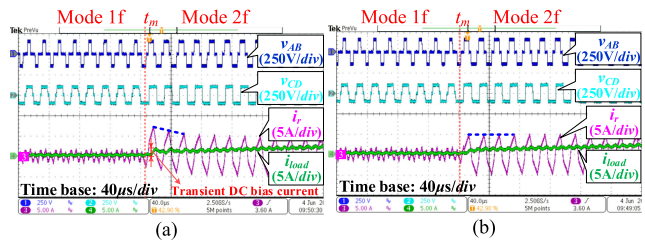

Fig. 19. Transient response from Mode 1f to Mode 2f. (a) Conventional TPS. (b) Universal modulation scheme without dc bias current.

Fig. 17 shows the transient response in Mode 2f, where the phase shift angle is switched from 0.19 π to 0.318 π at the time of t_m. In this case, the DAB converter works in forward power flow. Fig. 17(a) shows the conventional TPS in a transient state, where the transient dc bias current is positive. Fig. 17(b) shows the improved modulation scheme, which also actively demonstrates the effectiveness of the modulation scheme to suppress the transient dc bias current.

Fig. 18 shows the transient response in Mode 2r, where the phase shift angle is switched from $-0.19\ \pi$ to $-0.318\ \pi$ at the time of t_m. Fig. 18(a) shows the conventional TPS in a transient state. The transient dc bias current is negative because of the reverse power flow. Fig. 18(b) shows the improved modulation scheme without dc bias current in Mode 2r, which also actively demonstrates that the improved modulation scheme is also effective for reverse power flow in Mode 2r

Fig. 19 shows the transient response from Mode 1f to Mode 2f, where the phase shift angle is switched from 0.127 π to 0.255 π at the time of t_m. Fig. 19(a) shows the transient dc bias current for the conventional TPS control in the mode transition. Fig. 19(b) shows the improved modulation scheme without dc bias current. Although the working mode is transferred from Mode 1f to Mode2f, the universal modulation scheme to suppress the dc

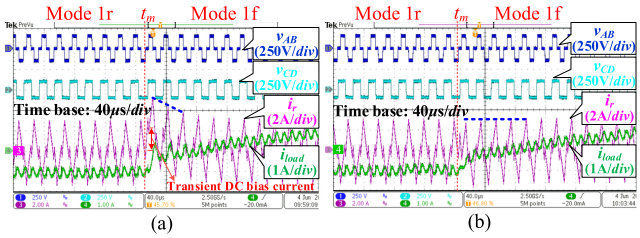

Fig. 20. Transient response from Mode 1r to Mode 1f. (a) Conventional TPS. (b) Universal modulation scheme without dc bias current.

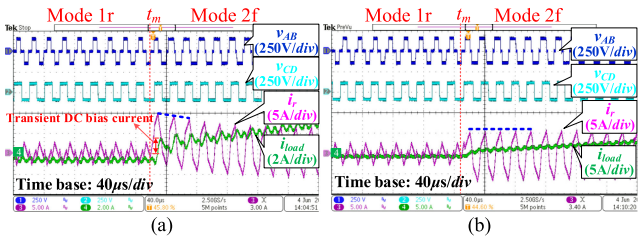

Fig. 21. Transient response from Mode 1r to Mode 2f. (a) Conventional TPS. (b) Universal modulation scheme without dc bias current.

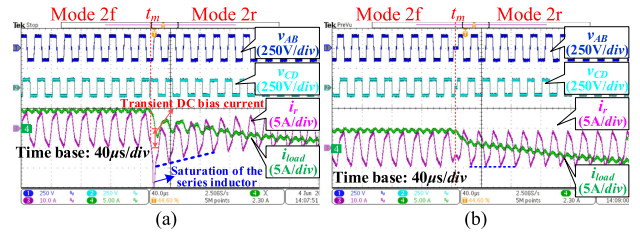

Fig. 22. Transient response from Mode 2f to Mode 2r. (a) Conventional TPS. (b) Universal modulation scheme without dc bias current.

bias current is effective without the need to select the working modes.

Fig. 20 shows the transient response from Mode 1r to Mode 1f, where the phase shift angle is switched from $-0.127\ \pi$ to $0.127\ \pi$ at the time of t_m. Fig. 20(a) also shows the transient dc bias current for the conventional TPS control. Fig. 20(b) shows the improved modulation scheme without dc bias current for the mode transition from Mode 1r to Mode 1f. In the mode transition from reverse power flow to the forward power flow, the transient dc bias current is still equal to zero.

Fig. 21 shows the transient response from Mode 1r to Mode 2f, where the phase shift angle is switched from $-0.127\ \pi$ to $0.318\ \pi$ at the time of t_m. Fig. 21(a) illustrates the dc bias current during the transient state. Fig. 21(b) further proves that the universal modulation scheme is effective for the mode transition from Mode 1r to Mode 2f.

Fig. 22 shows the transient response from Mode 1r to Mode 2f, where the phase shift angle is switched from $0.414\ \pi$ to $-0.414\ \pi$ at the time of t_m. Fig. 22(a) shows a large transient dc bias current because of a large error of the phase shift angle between the two adjacent switching periods. There is a large current spike in i_r, the current in the series inductor is not linear varied during the transient state, which demonstrates that the series inductor is inclined to be saturated. It may cause the overcurrent of the switches. Fig. 22(b) demonstrates that the universal modulation scheme can suppress the transient dc bias current even if the phase shift angle is switched by a large value. All the above experimental results validate the effectiveness of the universal modulation schemes. Because of the limitation of the article length, experimental results for other working mode transitions are not shown.

TABLE II
COMPARISONS OF TRANSIENT DC BIAS CURRENT ELIMINATION SCHEMES

	Proposed	[22]	[23]	[25]	[26]	[27]
Working modes	TPS	TPS	EPS	TPS	TPS	TPS
Global optimal working modes	Yes	No	No	No	No	No
ZVS in all the working modes	Yes	No	Yes	No	No	No
Unified algorithm during the transient states	Yes	No	No	No	No	No
Unified forward or reverse power cases	Yes	No	No	No	No	No
Complexity①	E	D	M	D	D	M

①E: easy; D: difficult; M: moderate

Table II presents the comparisons of the transient dc bias current elimination schemes. Most of the transient dc bias current elimination schemes are based on TPS. In TPS, there are three degrees of freedom. The duty cycle of the two full bridges and the phase shift angle are associated with the conduction loss and the soft-switching performance. Although most of the control schemes in Table II are based on TPS, only the proposed modulation scheme is suitable for the global optimal working modes with ZVS of all the switches and low current stress. Therefore, the converter by using the proposed modulation scheme can achieve minimum conduction loss and ZVS of all the switches in the wide conversion ratio. The control algorithms for different transient cases in the other scheme are different. In the forward and reverse power flow, the control algorithms are also different. Therefore, the transient cases, switching patterns or power conditions should be identified in the algorithm. In this article, the transient dc bias currents in all the working modes are unified in the same expression. Therefore, the proposed transient dc bias current elimination scheme is unified for all the transient cases and bidirectional power flow. There is no need to identify or select the transient cases or power conditions. The control algorithm is easy to be implemented.

V. CONCLUSION

In this article, a universal modulation scheme to suppress the transient dc bias current is proposed. The TPS can achieve global optimal control with minimum conduction loss and wide ZVS performance. The gate signals are updated once in a switching period, so the converter suffers from a large dc bias current during the transient state. By analyzing the dc bias current amplitude in the transient state, a modulation scheme without dc bias current is derived. The formulas to evaluate the transient dc bias current for the different working modes are the same, which demonstrates the modulation scheme to suppress the dc bias current can be unified. The implementation of the modulation scheme is proposed, which shows that the gate signals can be generated by the same strategy without the need to identify or

$$i_r(t)=\begin{cases} i_r(t_0)+\frac{V_{\rm in}-V_o/n}{L_r}(t-t_0) & (t_0\le t<t_{0m}) \quad t_0=0,\ t_{0m}=\frac{D_1T_s}{4} \\ i_r(t_{0m})+\frac{V_{\rm in}-V_o/n}{L_r}(t-t_{0m}) & (t_{0m}\le t<t_1) \quad t_1=\frac{D_1T_s}{2} \\ i_r(t_1)-\frac{V_o/n}{L_r}(t-t_1) & (t_1\le t<t_2) \quad t_2=\left(\frac{D_2}{2}+\frac{\varphi}{\pi}+\frac{D_1}{2}\right)\frac{T_s}{2} \\ i_r(t_2) & (t_2\le t<t_3) \quad t_3=\left(1-\frac{D_2}{2}+\frac{\varphi}{\pi}+\frac{D_1}{2}\right)\frac{T_s}{2} \\ i_r(t_3)+\frac{V_o/n}{L_r}(t-t_3) & (t_3\le t\le t_4) \quad t_4=\frac{T_s}{2} \end{cases} \tag{A1}$$

select the working modes or power conditions. Finally, the experimental prototype demonstrates that the universal modulation scheme to suppress the transient dc bias current is effective for all the working modes of the TPS.

APPENDIX

A1. Derivation of the Optimized Working Modes for Mode1f

The following derivation is taken Mode 1f for example. As seen in Fig. 2(a), the current at the commutating time can be expressed as (A1), as shown at the top of this page.

There is no dc bias current in the steady state, so $i_r(t_0)$ is equal to $-i_r(t_4)$. Therefore, the current at the commutating time is expressed as follows:

$$\begin{cases} i_r(t_0)=\frac{V_oT_s}{4nL_r}\left(\frac{2\varphi}{\pi}+D_1\right)-\frac{V_{\rm in}D_1T_s}{4L_r} \\ i_r(t_{0m})=\frac{V_oT_s}{4nL_r}\left(\frac{2\varphi}{\pi}\right) \\ i_r(t_1)=\frac{V_oT_s}{4nL_r}\left(\frac{2\varphi}{\pi}-D_1\right)+\frac{V_{\rm in}D_1T_s}{4L_r} \\ i_r(t_2)=-\frac{V_oD_2T_s}{4nL_r}+\frac{V_{\rm in}D_1T_s}{4L_r} \\ i_r(t_3)=-\frac{V_oD_2T_s}{4nL_r}+\frac{V_{\rm in}D_1T_s}{4L_r} \\ i_r(t_4)=-\frac{V_oT_s}{4nL_r}\left(\frac{2\varphi}{\pi}+D_1\right)+\frac{V_{\rm in}D_1T_s}{4L_r}. \end{cases} \tag{A2}$$

The output power can be expressed as

$$P_o=\frac{V_{\rm bat}V_oT_s}{nL_r}\frac{\varphi}{2\pi}D_1. \tag{A3}$$

To make the tradeoff between the conduction loss and ZVS of all the switches in Mode 1f, the following constraints should be met: $i_r(t_0)\le -I_{\rm ZVS\,1}$, $i_r(t_1)\ge I_{\rm ZVS1}$, and $i_r(t_2)/n=i_r(t_3)/n\le -I_{\rm ZVS2}$. The peak current of the transformer is $i_r(t_1)$. If the peak current in the transformer is reduced, the conduction loss also can be reduced. Setting the peak current as the control objective, the optimization formulas with the minimum conduction loss and the ZVS conditions are defined as

$$\begin{cases} \mathrm{Min}[i_r(t_1)] \\ \text{Subject to } P_o(D_1,D_2,\varphi)=p* \\ i_r\left(t_0\right)\le -I_{\rm ZVS1} \\ i_r\left(t_3\right)/n\le -I_{\rm ZVS2} \end{cases} \tag{A4}$$

where p^* is the desired nominal output power. According to (A4), the evaluation function can be expressed as

$$\begin{aligned} f\left(D_1,D_2,\varphi\right)=&\ i_r(t_1)+\lambda\left(P_n-p^*\right)+\mu\left(i_r\left(t_0\right)+I_{\rm ZVS1}\right) \\ &+\sigma\left(i_r\left(t_3\right)/n+I_{\rm ZVS2}\right). \end{aligned} \tag{A5}$$

Solving (A5), when D_1 and D_2 are expressed in (2), $f\,(D_1,\ D_2,\ \varphi)$ gets the minimum value.

For the other working modes in Fig. 2, the control law for the minimum conduction loss and the ZVS conditions can be derived in a similar method. Therefore, the expression in (3) to (5) can be derived.

REFERENCES

[1] Z. Guo, K. Sun, T. Wu, and C. Li, "An improved modulation scheme of current-fed bidirectional DC-DC converters for loss reduction," *IEEE Trans. Power Electron.*, vol. 33, no. 5, pp. 4441–44457, May 2018.

[2] Y. R. Kafle, S. U. Hasan, and G. E. Town, "Quasi-Z-source based bidirectional DC-DC converter and its control strategy," *Chin. J. Elect. Eng.*, vol. 5, no. 1, pp. 1–10, Mar. 2019.

[3] M. H. Kheraluwala, R. W. Gascoigne, D. M. Divan, and E. D. Baumann, "Performance characterization of a high-power dual active bridge dc-to-dc converter," *IEEE Trans. Ind. Appl.*, vol. 28, no. 6, pp. 1294–1301, Nov./Dec. 1992.

[4] P. Liu, C. Chen, S. Duan, and W. Zhu, "Dual phase-shifted modulation strategy for the three-level dual active bridge DC–DC converter," *IEEE Trans. Ind. Electron.*, vol. 64, no. 10, pp. 7819–7830, Oct. 2017.

[5] B. Zhao, Q. Yu, and W. Sun, "Extended-phase-shift control of isolated bidirectional DC–DC converter for power distribution in microgrid," *IEEE Trans. Power Electron.*, vol. 27, no. 11, pp. 4667–4680, Nov. 2012.

[6] F. Krismer and J. W. Kolar, "Closed form solution for minimum conduction loss modulation of DAB converters," *IEEE Trans. Power Electron.*, vol. 27, no. 1, pp. 174–188, Jan. 2012.

[7] B. Zhao, Q. Song, and W. Liu, "Efficiency characterization and optimization of isolated bidirectional DC–DC converter based on dual-phase-shift control for DC distribution application," *IEEE Trans. Power Electron.*, vol. 28, no. 4, pp. 174–188, Apr. 2013.

[8] N. Hou, W. Song, and M. Wu, "Minimum-current-stress scheme of dual active bridge DC–DC converter with unified phase-shift control," *IEEE Trans. Power Electron.*, vol. 31, no. 12, pp. 8552–8561, Dec. 2016.

[9] G. Xu, L. Li, X. Chen, Y. Liu, Y. Sun, and M. Su, "Optimized EPS control to achieve full load range ZVS with seamless transition for dual active bridge converters," *IEEE Trans. Ind. Electron.*, vol. 68, no. 9, pp. 8379–8390, Sep. 2021.

[10] J. Huang, Y. Wang, Z. Li, and W. Lei, "Unified triple-phase-shift control to minimize current stress and achieve full soft-switching of isolated bidirectional DC–DC converter," *IEEE Trans. Ind. Electron.*, vol. 63, no. 7, pp. 4169–4179, Jul. 2016.

[11] A. Tong, L. Hang, G. Li, X. Jiang, and S. Gao, "Modeling and analysis of a dual-active-bridge-isolated bidirectional DC/DC converter to minimize RMS current with whole operating range," *IEEE Trans. Power Electron.*, vol. 33, no. 6, pp. 174–188, Jun. 2018.

[12] Z. Guo, "Modulation scheme of dual active bridge converter for seamless transitions in multiworking modes compromising ZVS and conduction loss," *IEEE Trans. Ind. Electron.*, vol. 67, no. 9, pp. 7399–7409, Sep. 2020.

[13] B. Zhao, Q. Song, W. Liu, G. Liu, and Y. Zhao, "Universal high-frequency-link characterization and practical fundamental-optimal strategy for dual-active-bridge dc-dc converter under PWM plus phase-shift control," *IEEE Trans. Power Electron.*, vol. 30, no. 12, pp. 6488–6494, Dec. 2015.

[14] Z. Xiao, Z. He, H. Wang, A. Luo, Z. Shuai, and J. M. Guerrero, "General high-frequency-link analysis and application of dual active bridge converters," *IEEE Trans. Power Electron.*, vol. 35, no. 8, pp. 8673–8688, Aug. 2020.

[15] H. Shi, H. Wen, Y. Hu, and L. Jiang, "Reactive power minimization in bidirectional DC–DC converters using a unified-phasor-based particle swarm optimization," *IEEE Trans. Power Electron.*, vol. 33, no. 12, pp. 10990–11006, Dec. 2018.
[16] D. Segaran, D. G. Holmes, and B. P. McGrath, "Enhanced load step response for a bidirectional DC–DC converter," *IEEE Trans. Power Electron.*, vol. 32, no. 3, pp. 1964–1974, Mar. 2017.
[17] H. Bai, C. Mi, C. Wang, and S. Gargies, "The dynamic model and hybrid phase-shift control of a dual-active-bridge converter," in *Proc. 34th Annu. Conf. IEEE Ind . Electron.*, 2008, pp. 2840–2845.
[18] W. Song, N. Hou, and M. Wu, "Virtual direct power control scheme of dual active bridge DC–DC converters for fast dynamic response," *IEEE Trans. Power Electron.*, vol. 33, no. 2, pp. 1750–1759, Feb. 2018.
[19] N. Hou, W. Song, Y. Li, Y. Zhu, and Y. Zhu, "A comprehensive optimization control of dual-active-bridge DC–DC converters based on unified-phase-shift and power-balancing scheme," *IEEE Trans. Power Electron.*, vol. 34, no. 1, pp. 826–839, Jan. 2019.
[20] B. Zhao, Q. Song, W. Liu, and Y. Zhao, "Transient DC bias and current impact effects of high-frequency-isolated bidirectional DC–DC converter in practice," *IEEE Trans. Power Electron.*, vol. 31, no. 4, pp. 3203–3216, Apr. 2016.
[21] S. Wei, Z. Zhao, K. Li, L. Yuan, and W. Wen, "Deadbeat current controller for bidirectional dual-active-bridge converter using an enhanced SPS modulation method," *IEEE Trans. Power Electron.*, vol. 36, no. 2, pp. 1274–1279, Feb. 2021.
[22] Q. Bu, H. Wen, J. Wen, Y. Hu, and Y. Du, "Transient DC bias elimination of dual-active-bridge DC–DC converter with improved triple-phase-shift control," *IEEE Trans. Ind. Electron.*, vol. 67, no. 10, pp. 8687–8598, Oct. 2020.
[23] T. Dai *et al.*, "Research on transient DC bias analysis and suppression in EPS DAB DC-DC converter," *IEEE Access*, vol. 8, pp. 61421–61432, 2020.
[24] G. Ortiz, J. Mühlethaler, and J. W. Kolar, "'Magnetic ear'-based balancing of magnetic flux in high power medium frequency dual active bridge converter transformer cores," in *Proc. 8th Int. Conf. Power Electron*, 2011, pp. 1307–1314.
[25] C. Yang, J. Wang, C. Wang, X. You, and X. Lei, "Transient DC bias current reducing for bidirectional dual active bridge DC-DC converter by modifying modulation," *IEEE Trans. Power Electron.*, vol. 36, no. 11, pp. 13149–13161, Nov. 2021.
[26] S. Wang, C. Li, K. Wang, Z. Zheng, and Y. Li, "Loss imbalance and transient dc-bias mitigation in dual active bridge dc/dc converters," *IEEE J. Emerg. Sel. Topics Power Electron.*, vol. 9, no. 2, pp. 1399–1409, Apr. 2021.
[27] J. Hu, S. Cui, D. V. D. Hoff, and R. W. De Doncker, "Generic dynamic phase-shift control for bidirectional dual-active bridge converters," *IEEE Trans. Power Electron.*, vol. 36, no. 6, pp. 6197–6202, Jun. 2021.

Shujun Mu was born in 1984. He received the B.S. degree in electrical engineering from Shandong University, Jinan, China, in 2007, the M.S. degree from the Huazhong University of Science and Technology, Wuhan, China, in 2009, and the Ph.D. degree from Tsinghua University, Beijing, China, in 2015.

He is currently an Engineer with the National Institute of Clean and Low Carbon Energy, Beijing, China. His research interests include hydrogen integration and control, power electronic systems, and electromagnetic design of motors and generators

Zhiqiang Guo (Member, IEEE) received the B.S. degree in automation from Hebei University of Technology, Tianjin, China, in 2008, and the M.S. and Ph.D. degrees in electrical engineering from Beijing Institute of Technology, Beijing, China, in 2010 and 2015, respectively.

From 2015 to 2017, he was a Postdoctoral Research Fellow with the Department of Electrical Engineering, Tsinghua University, Beijing, China. In 2017, he joined the Faculty of School of Automation, Beijing Institute of Technology, where he is currently an Assistant Professor. He has authored more than 30 papers and two books in the field of power electronics. His current research interests include dc–dc converters, distributed generation, and microgrid applications.

Yong Luo received the B.S. degree in electrical engineering in 2019 from Beijing Institute of Technology, Beijing, China, where he is currently working toward the M.S. degree.

His current research interests include the topology and modeling of dc–dc converters, control and modeling of the bidirectional dc–dc converters, and switching supply.